Hindawi Publishing Corporation
Advances in Materials Science and Engineering
Volume 2014, Article ID 127531, 10 pages
http://dx.doi.org/10.1155/2014/127531

Research Article

Templateless Synthesis and Characterization of Hollow Gadolinium Doped Cerium Oxide Nanofibers by Electrospinning

Chutima Thiabdokmai,[1] Apishok Tangtrakarn,[2,3,4,5] Shatchai Promsuy,[2,5] Pilan Ngiewlay,[1] and Charusporn Mongkolkachit[6]

[1] *Materials Science and Nanotechnology Program, Faculty of Science, Khon Kaen University, Khon Kaen 40002, Thailand*
[2] *Department of Physics, Faculty of Science, Khon Kaen University, Khon Kaen 40002, Thailand*
[3] *Nanotec-KKU Center of Excellence on Advanced Nanomaterials for Energy Production and Storage, Khon Kaen University, Khon Kaen 40002, Thailand*
[4] *Thailand Center of Excellence in Physics, CHE, Ministry of Education, Bangkok 10400, Thailand*
[5] *Integrated Nanotechnology Research Center, Khon Kaen University, Khon Kaen 40002, Thailand*
[6] *National Metal and Materials Technology Center (MTEC), Khlong Nueng, Khlong Luang, Pathumthani 12120, Thailand*

Correspondence should be addressed to Apishok Tangtrakarn; nateta@kku.ac.th

Received 8 January 2014; Revised 20 April 2014; Accepted 28 April 2014; Published 2 June 2014

Academic Editor: Markku Leskela

The hollow nanofibers of $Ce_{0.8}Gd_{0.2}O_{2-\delta}$ (GDC20) were electrospun from the PVP and nitrate precursors. The evolution of hollow channel was investigated by TG-DTA and ex situ TEM for the fibers heated at 250–300°C for 1–5 h. The hollow cores were revealed during the crystallization of nano-GDC20 and the PVP decomposition stage. The structural and morphological properties of GDC20 fibers before and after being calcined at 500–900°C for 8 h were investigated by FTIR, FE-SEM, TEM, EDS, XRD, and Raman spectroscopy. The results from XRD and Raman scattering verify the successful doping of Gd^{3+} ions into the CeO_2 host lattice. The conductivity of the cold-pressed GDC 20 pellet sintered at 1400°C is more than 0.01 S/cm at and above 600°C.

1. Introduction

Cerium oxide (CeO_2) has drawn much attention because of its wide spectrum of applications such as components in a solid oxide fuel cell (SOFC), an oxygen sensor, an exhaust catalyst [1–4], and so forth. Doping CeO_2 with rare-earth elements has been universally adopted to tune ceria performances since their electrical conductivity, catalytic activity, and optical property were altered with changes in oxygen vacancies [5–7]. Cerium oxide bulks with gadolinium dopants of around 10–20% (GDCX, X = 10–20%) were reported to achieve promising ionic conductivity at intermediate temperatures ranging from 500 to 750°C [8–10], and thus they are a leading candidate for an SOFC electrolyte. It is worth noting that, in order to reduce a cathode polarization resistance of an SOFC, an electrolyte material, such as GDC, is also required to be present in an SOFC cathode for transporting oxygen ions to the SOFC electrolyte part and supporting the other mixed ionic-electronic conducting material which acts as a catalyst for oxygen reduction and electron transportation.

Various methods have been used to prepare GDC with interesting nanofeatures such as combustion process [7, 11], sol gel synthesis [12], coprecipitation [7, 13], hydrothermal synthesis [14], and electrospinning [15]. Comparing to other techniques, electrospinning is a remarkable process employed to create a long 1D nanostructure. The derived nanofibers have large surface areas which offer the great number of active sites for catalytic reactions to occur. For this reason, including GDC nanofibers in the SOFC electrodes can enhance the SOFC performance because numerous open channels created among the overlaid fibers can give pathways for a gas flux to reach reaction sites.

In this study, hollow GDC nanofibers were fabricated to increase active areas over the conventional solid version. Furthermore, the hollow core could open the possibility

for insertion of another functional material. Generally, the absence of material at the center of electrospun nanofibers can be induced by removing the sacrificial core layer such as oil [16, 17]. Alternatively, it is possible for the virgin cerium oxide nanofibers to be prepared without the use of any sacrificial layer as previously proposed by Qizheng et al. [18]. It was hypothesized that the migration of Ce^{3+} to the fiber surface during the water evaporation, the subsequent decomposition of PVP, and oxidation of Ce^{3+} ion are mechanisms responsible for nanohole formation. Here, we also reinvestigated this hypothesis with TG-DTA and ex situ TEM on our prepared GDC20 fibers. Furthermore, the impact of heat treatment on selected structural properties and the morphology of these nanofibers were investigated. According to our literature reviews, GDC nanofibers are rarely investigated for their electrical properties so the temperature-dependent conductivity measurement was carried out using an ac-impedance technique as well.

2. Experimental

The nanofibers of GDC20 were prepared from the mixture between polyvinylpyrrolidone (PVP) ($M_n \approx 360{,}000$, Aldrich), ethyl alcohol (10 wt%), nitrate solutions, and N,N-dimethylformamide (DMF). The stoichiometric weight of $Gd(NO_3)_3{\cdot}6H_2O$ (Aldrich, 99.90%) and $Ce(NO_3)_3{\cdot}6H_2O$ (Aldrich, 99.99%) were thoroughly dissolved in DI-H_2O and DMF to obtain a 0.26 M solution. Then proper amounts of nitrates and PVP solution were mixed together and vigorously stirred for 24 h. The derived yellow solution was loaded into a syringe with 22-gage needle for the electrospinning process. The nitrate-PVP nanofibers were collected on a flat Al-foil covered plate. A working distance and an applied voltage were fixed at 20 cm and 14 kV, respectively. The nonwoven as-spun fibers were dried at 80°C for several hrs and subjected to thermogravimetric/differential thermal analysis (TG/DTA, Perkin Elmer TGA7, USA). The heating rate for TG/DTA and all thermal treatment were maintained at 5°C/min. Fourier transform infrared spectroscopy (FTIR, Nicolet Nexus 670, USA) was used to study the functional groups of as spun fibers as well as those calcined for 8 h at 500, 600, 700, 800, and 900°C. The formation of holes was specifically studied with a transmission electron microscopy (TEM, FEI/Tecnai G2 20, USA) for fibers heated from 1 to 6 h at 250, 275, and 300°C. All calcined nanofibers (500–900°C, 8 h) were also characterized for their morphological change with TEM and field-emission scanning electron microscopy (FESEM, JEOL JSM-6335F, Japan). The crystal structure and crystallinity of calcined nanofibers were analyzed using X-ray diffraction techniques (XRD, PANalytical, The Netherlands) and selected-area electron diffraction- (SEAD-) TEM. The composition of the GDC20 fiber was identified with energy dispersive spectroscopy (EDS, JEOL JSM-6335F, Japan). To study the impact of % content of Gd dopant (x) on the lattice parameter and crystallite size of CeO_2, additional samples of $Ce_{1-x}Gd_xO_{2-\delta}$ with x varied from 5 to 15% were also prepared. Apart from XRD, Raman spectroscopy (Raman, Jobin Yvon Horiba T-64000, France) was used to verify the successful incorporation of Gd into the CeO_2 host lattice and the generation of oxygen vacancies. Moreover, Gd_2O_3 was also prepared and used as an impurity reference. For electrochemical impedance spectroscopy (EIS) testing, a Solartron 1260 frequency response analyzer (Solartron, UK) set in the frequency range from 0.1 Hz to 5 MHz and with a perturbation AC of 100 mV was used. Samples for EIS testing were made by cold pressing ground fibers at 1 ton and subsequently sintering the pellets (1 cm in a diameter) at 1400°C for 4 h to get dense bulks suitable for the conductivity measurement. Pt wires and Pt paste were used as current collectors. The conductivity measurements were carried out from 250 to 800°C.

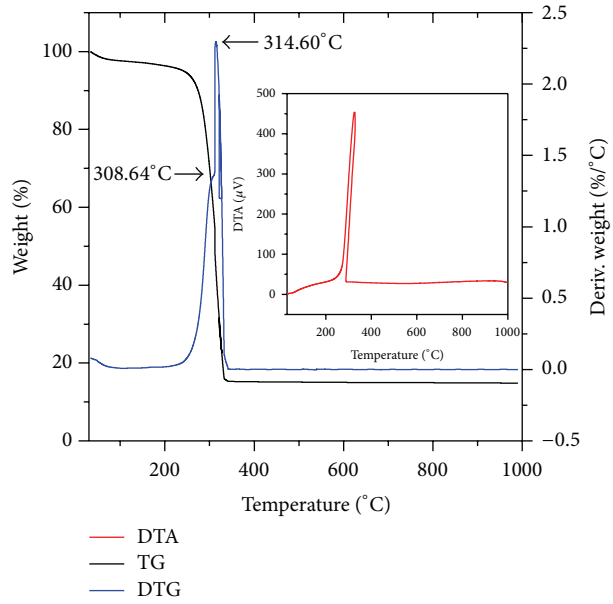

Figure 1: TG/DTG curves with DTA inset of $Ce(NO_3)_3/Gd(NO_3)_3$/PVP composite nanofibers at a heating rate of 5°C/min in static air.

3. Results and Discussion

3.1. Thermogravimetric and Differential Thermal Analysis (TG/DTA). The TG/DTA was used to study thermal decomposition and combustion of $Ce(NO_3)_3/Gd(NO_3)_3$/PVP nanofibers. TG/DTA results were shown in Figure 1. The TG curve shows three steps of weight losses. The initial weight loss of 5.48% in the temperature range between 30 and 250°C corresponds to the evaporation of the moisture and solvents in composite fibers. In this initial stage, PVP is thermally stable. The second set of weight loss of 39.52%, taking place between 250 and 310°C, is related to the decomposition of nitrate compounds and the break of PVP side chains. The last weight loss of 41%, occurring in the range of 310–330°C, is mainly due to the thermal decomposition of PVP main chains [18]. From DTA results (Figure 1 inset), the strong combustion of PVP occurs at ~324°C. If the heating temperature is increased above 330°C, the TG and DTA curve barely changed, indicating that water, organic compounds, and nitrates in composite fibers are burned off. The total weight

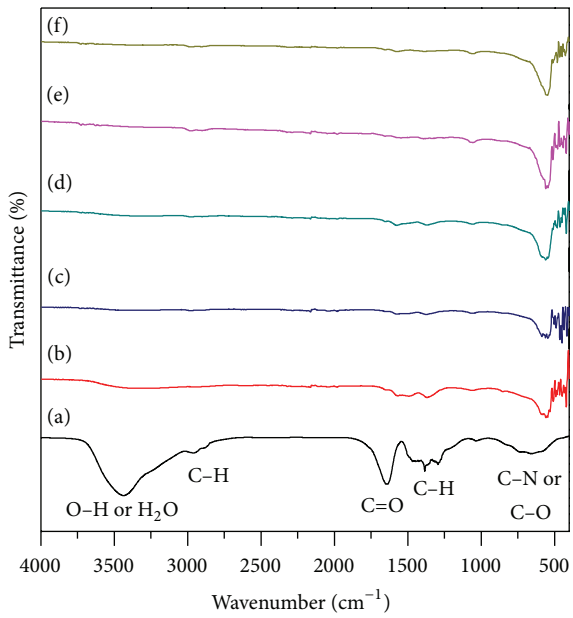

FIGURE 2: FTIR spectra of GDC20 before (a) and after calcination at (b) 500°C, (c) 600°C, (d) 700°C, (e) 800°C, and (f) 900°C for 8 h in air.

loss from the beginning is approximately 86%, leaving the remnant weight of 14%, which mostly belongs to the GDC20 ceramic [7, 18].

3.2. Fourier Transformed Infrared (FT-IR). The FT-IR spectra of as-spun nanofibers and those calcined at 500–900°C for 8 h in air are shown in Figure 2. The absorption bands located at around 3479, 2963, 1643, 1367, and 1060 cm^{-1} belong to PVP. The large band at ~3479 cm^{-1} signifies the presence of residual water, which has stretching vibrations of hydroxyl group (ν_{O-H}) [15–18]. Residual organics in the sample have the bands between 2963 and 1060 cm^{-1}. The band at ~2963 and 2874 cm^{-1} are matched to the C–H stretching mode (ν_{C-H}). The band at ~1643 cm^{-1} corresponds to the carbonyl group ($\nu_{C=O}$) [15, 16]. The band at ~1367 cm^{-1} represents C–H bond (ν_{C-H}) [7]. The less intense peak at ~1060 cm^{-1} is related to C–N (ν_{C-N}) and/or C–O (ν_{C-O}). It is clear from Figure 2 that all the residual peaks become weaken right from 500°C as most organics are burned off, resulting in the full oxidation of cerium, so Ce–O stretching modes lower than 500 cm^{-1} appear at all temperatures [19, 20]. The slight amount of residual carbon is detected in FTIR results for samples sintered at 500°C, even though the carbon should not exist above 330°C according to TG/DTA. This difference should come from the fact that only a small amount of sample was used for the TG/DTA testing, therefore; therefore carbon residues were easily oxidized. In the real situation, with larger sample quantity, carbon soot may not be totally cleaned. Furthermore, carbon and humidity contamination from the environment do easily occur in the ceria samples.

3.3. Field Emission Scanning Electron Microscope (FESEM). The morphologies of as-spun and GDC20 nanofibers calcined at different temperatures were shown in Figure 3. The FESEM images reveal the smooth surface of continuous as-spun nanofibers with the diameter of 311.6 ± 80.56 nm. The outer diameters of nanofibers after being calcined at 500, 600, 700, 800, and 900°C (averaged from over 300 strands) are 87.25 ± 9.03 nm, 74.79 ± 5.87 nm, 66.30 ± 10.36 nm, 59.85 ± 5.50 nm, and 51.85 ± 5.85 nm, respectively. The shrinkage of fiber could correspond to the coalescenceof grains during the sintering process. Figures 3(b)–3(d) confirm the presence of the hollow core. The origin and evolution mechanism of holes were subjected to further investigation with TEM analysis.

3.4. Transmission Electron Microscopy (TEM). The formation of hollow channel was examined by TEM. Figures 4 and 5 show certain TEM bright field images and selected-area electron diffraction (SAED) patterns of GDC20 fibers after selected heat treatments. The change in the GDC20 fiber morphology after being heated at 250–300°C for 1–5 h in air was shown in Figure 4. It is clear that the as-spun fibers have no channels at their centers. The appearance of core takes place around 5 h, 3 h, and 1 h for fibers heated at 250, 275, and 300°C, respectively. The time required to create the hollow center at 300°C is 4-5 times less than what is required for 250°C. Therefore, increasing the heating temperature will accelerate the hole-formation process. By referring to TG/DTA results, the evolution of these nanocores, which occurs at around 250–300°C, is associated with the decomposition of the nitrates and polymer matrix. The decomposition of PVP does not lead to the collapse of the nanofibers because the crystallized oxidized Ce-Gd nanoparticles on the outer perimeter of the nanofibers help sustain the nanofiber structure since the nanofibril bridges, belonged to the PVP remnants, across the inner shell of fibers were observed (Figure 4(c)). The presence of the hollow core during the decomposition of the polymer matrix and crystallization of CeO_2 matches the hypothesis proposed by Qizheng et al. The crystallization of nanoscale GDC20 is confirmed by the appearance of sharp circular rings in the SAED pattern. The inset SAED images in Figures 4(c), 4(e), and 4(f) reveal that the crystallization of nano-GDC already takes place after heating the fibers at 250, 275, and 300°C for 5, 3, and 1 h, respectively. Moreover, as compared to as-spun fibers, the outer diameters of heated fibers obviously become smaller because large portions of polymer are burnt-off. During this step, the metal nitrates could migrate further toward the outer perimeter of fibers, which is opposite to oxidation direction of metal complexes which go toward the fiber center.

The fibers were subjected to higher heating temperatures to check on the stability of the hollow cores. Figure 5 shows TEM bright field images and SAED patterns of GDC20 nanofibers (inset) before and after being calcined at 500–900°C for 8 h in air. All fibers become crystallized due to the presence of spotty ring patterns in SEAD results. The hollow cores of fibers still exist from 500 to 800°C but disappear at 900°C as all grains enlarge and completely fill up the channels. From TEM, the average grain size of fibers is 8.64 ± 3.63 nm, 12.83 ± 4.62 nm, 20.21 ± 5.21 nm, 31.07 ± 10.67 nm, and

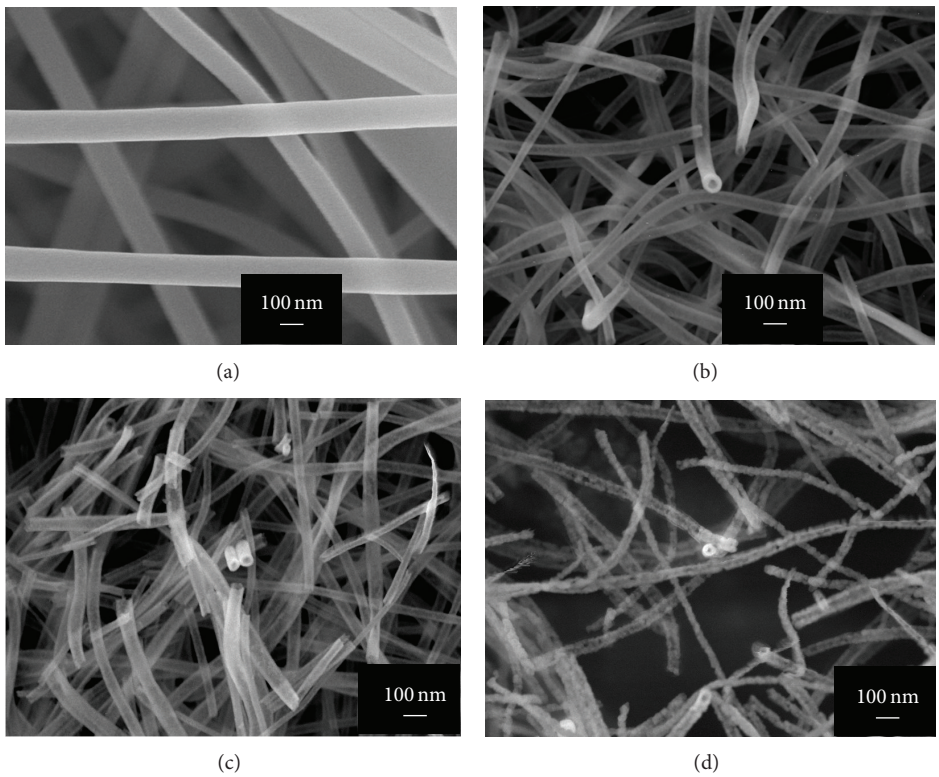

Figure 3: FESEM images of the GDC20 for (a) as-spun nanofibers and those calcined at (b) 500°C, (c) 700°C, and (d) 800°C for 8 h in air.

42.35 ± 13.48 after subjected to a calcination temperature of 500, 600, 700, 800, and 900°C, respectively.

3.5. Energy Dispersive Spectroscopy (EDS). The energy dispersive spectroscopy (EDS) in SEM was used to determine the composition of Ce and Gd of GDC20 nanofibers after being calcined at 800°C for 8 h in air. The GDC20 fibers were attached to aluminum stub with carbon tapes. The ratio of Gd and Ce derived from Ce-L and Gd-L lines is ~4 to 1.

3.6. X-Ray Diffraction (XRD). The crystal structure, grain size, and the lattice parameter of grounded cerium oxide (CeO_2) and GDC20 nanofibers were analyzed from XRD spectra. The XRD patterns of GDC20 nanofibers calcined at 500–900°C for 8 h in air are shown in Figure 6. Comparing to JCPDS number 75-0162 [7], the crystal structure of all calcined nanofibers is a cubic fluorite [21, 22]. The crystallite size of calcined CeO_2 and GDC20 were determined using Scherrer's equation: $D = k\lambda/\beta\cos\theta$, where k is 0.89, λ is the wavelength of X-ray source ($\lambda = 1.54065$ Ang.), β is the full width at half maximum of a (111) peak, and θ is Bragg's diffraction angle. Figure 7(a) shows the trend of increasing crystallite size with the increasing temperature due to a sintering effect. From XRD, the average crystallite size of GDC20 fiber is 8.33 ± 2.98 nm, 13.26 ± 4.62 nm, 21.45 ± 2.14 nm, 31.94 ± 4.10 nm, and 43.84 ± 5.63 nm, respectively. It was found that the values of crystal size from TEM and XRD match rather well, so the results from XRD were used for studying the effect of %Gd dopant on the crystal growth of CeO_2. From Figure 7, the crystallite sizes of CeO_2 and GDC20 are still retained in nanoregime even at 900°C. Furthermore, it is found that Gd doping reduces the grain growth of CeO_2. This trend is also reported by Hernández et al. [5]. A simple explanation for such phenomena is the impediment of Ce movement with the presence of Gd atoms. The effect of calcination temperature toward the lattice parameter of CeO_2 and GDC20 nanofibers was shown in Figure 7(b). The lattice parameters of both CeO_2 and GDC20 are not significantly altered within the heating range of 500–900°C, confirming the good stability of the materials. The lattice parameter of GDC20 which falls between 5.420 and 5.423 angstroms is still close to those obtained from JCPDS card number (75-0162). The variation of a lattice parameter with a Gd dopant content was selectively investigated and used as implication for the formation of solid solution between the Gd and the CeO_2. Since Gd^{3+} (0.105 nm) radius is larger Ce^{4+} (0.097 nm), the replacement of Gd on Ce site will lead to an expansion of the Ce host lattice, leading to a shift in 2θ. As shown in Figure 8(a), the unit cell parameter (a) increases with the dopant content (x%). The fitting of x-a curve data shows a linear relationship following the equation as $a_{\text{our work}} = 0.000664x + 5.4099$. According to Vegard's rule, the linear relationship between the lattice parameter and the dopant (x%) implies the creation of GDC solid solution. From Figure 8(b), it is shown that the crystallite size decreases with the increasing Gd^{3+} concentration [22]. This grain growth retardation phenomenon also provides the evidence that Gd doping is achieved.

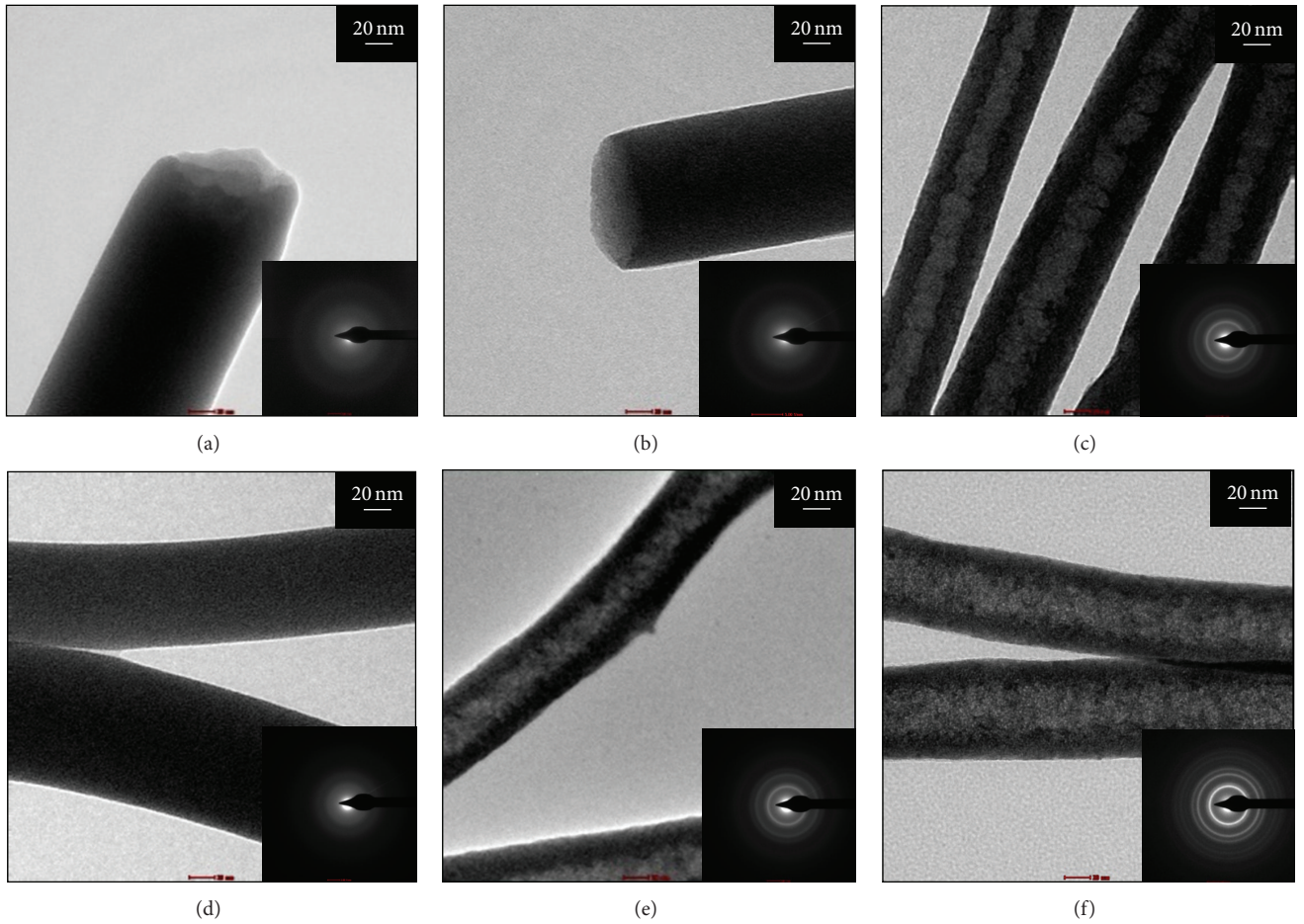

Figure 4: TEM bright field images of GDC20 nanofibers for (a) as-spun sample and those heated at (b) 250°C 3 h, (c) 250°C 5 h, (d) 275°C 1 h, (e) 275°C 3 h, and (f) 300°C 1 h in air and their associated selected area electron diffraction (SAED) patterns: inset.

3.7. Raman Spectroscopy. Figure 9 shows the Raman spectra of CeO_2 (Figure 9(a)) and GDC20 (Figure 9(b)) samples calcined at different temperatures (500, 600, 700, 800, and 900°C). The Raman spectrum of CeO_2 calcined at 500°C was used as a reference (Figure 9(b)-inset). Using 532.14 nm laser lines, the intense peak of CeO_2 due to F_{2g} symmetry of oxygen around cerium ion locates at 465 cm^{-1} [15]. The absence of Gd_2O_3 peak at 360 cm^{-1} confirms a good stability of Gd in the ceria lattice between 500 and 900°C [23].

In Figure 9, CeO_2 annealed at the same condition was compared to GDC20. The F_{2g} peak of GDC20 is broader than that of CeO_2 because Gd doping causes the disorder in the oxygen sublattice. The shift of F_{2g} peak to the lower frequency (460 cm^{-1}) was observed for the GDC20 as compared to 464 cm^{-1} of CeO_2. The lowering phonon energy (red shift) and the broadening of the GDC 20 relate to the lattice expansion of CeO_2 from a successful incorporation of Gd [15]. These Raman results correspond well with those obtained from XRD.

For GDC 20, two additional peaks observed at 550 and 600 cm^{-1} are related to the oxygen vacancies in nanocrystalline GDC20 sample [24]. These oxygen vacancies are responsible for the ionic conductivity in the GDC20. The mode at 550 cm^{-1} (alpha peak), associated with the extrinsic oxygen vacancy, is induced by the doping of CeO_2 with Gd^{3+} [7], following the equation:

$$Gd_2O_3 + 2Ce_{Ce}^{x} + O_O^{x} \longrightarrow 2Gd'_{Ce} + \ddot{V}_O + 2CeO_2 \quad (1)$$

From Figure 9(b), the alpha peak increases with the increasing temperature. Such phenomenon was also reported by Li et al. [24] for the 325 nm Raman laser, which is more sensitive to the surface defects. However, when they used 514 nm laser, their alpha peak does not noticeably change with the increasing temperature, which is different to our results. In our case, laser 532.14 nm was used, so the large portion of laser goes deeper into the bulk. This means that the concentration of oxygen vacancy created from Gd doping in our case also occurs deeper in the bulk region. Such variation could be related to the difference in a material fabrication process. Another vacancy peak at 600 cm^{-1} (beta peak) belongs to the oxygen vacancy neighboring or the GdO_8-type defect complex. Similar to results from Li et al., the beta peak decreases with the rising temperature because there are

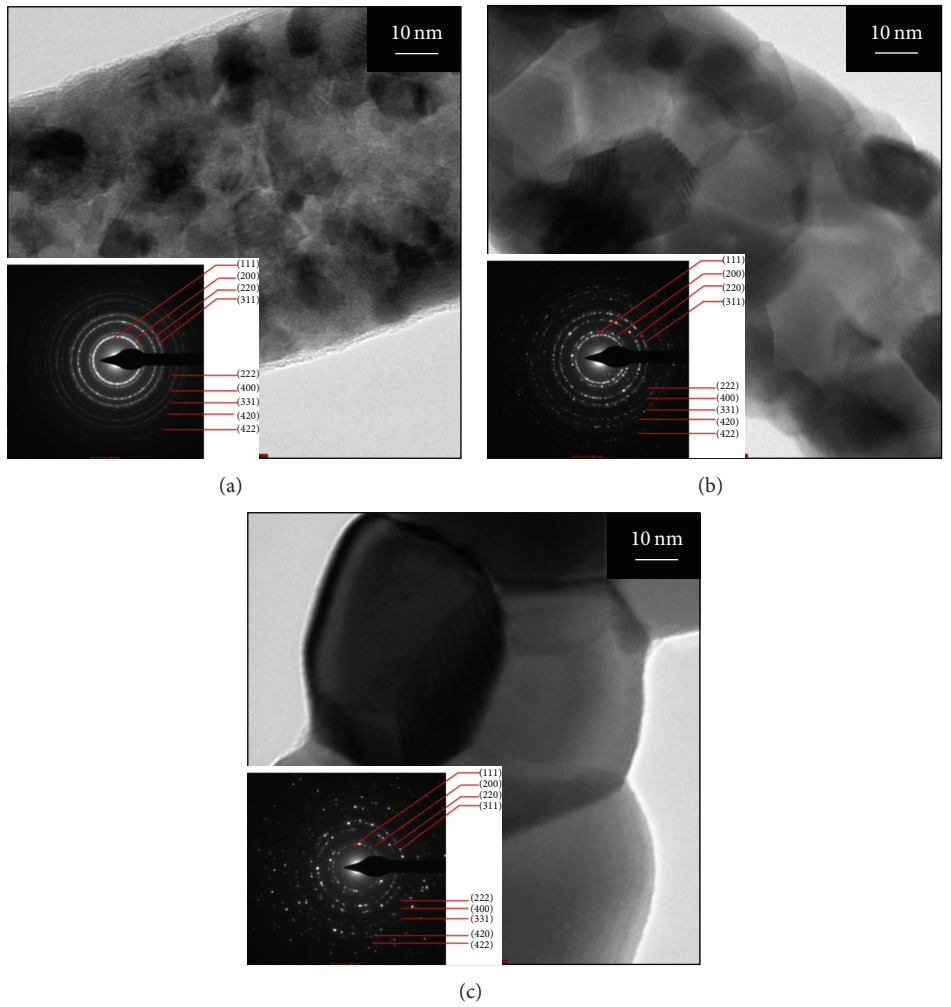

Figure 5: TEM bright field images and selected area electron diffraction (SAED) patterns of GDC20 nanofibers calcined in air at different temperature for (a) 500°C, (b) 700°C, and (c) 900°C for 8 h.

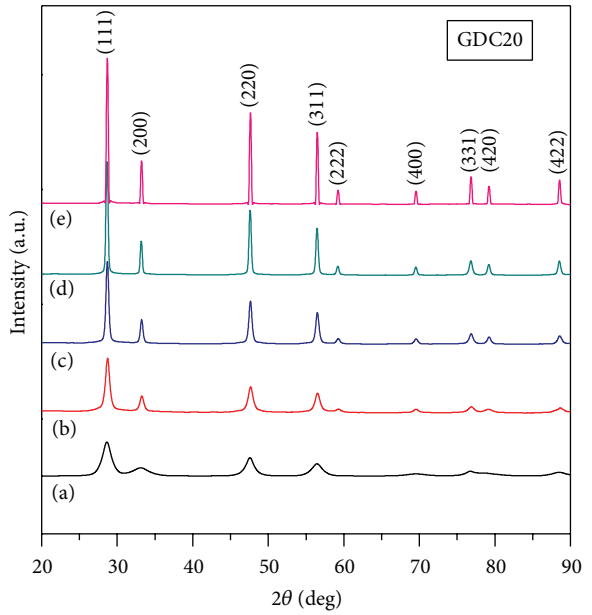

Figure 6: X-ray diffraction patterns of GDC20 nanofibers calcined at different temperature for (a) 500°C, (b) 600°C, (c) 700°C, (d) 800°C, and (f) 900°C for 8 h in air.

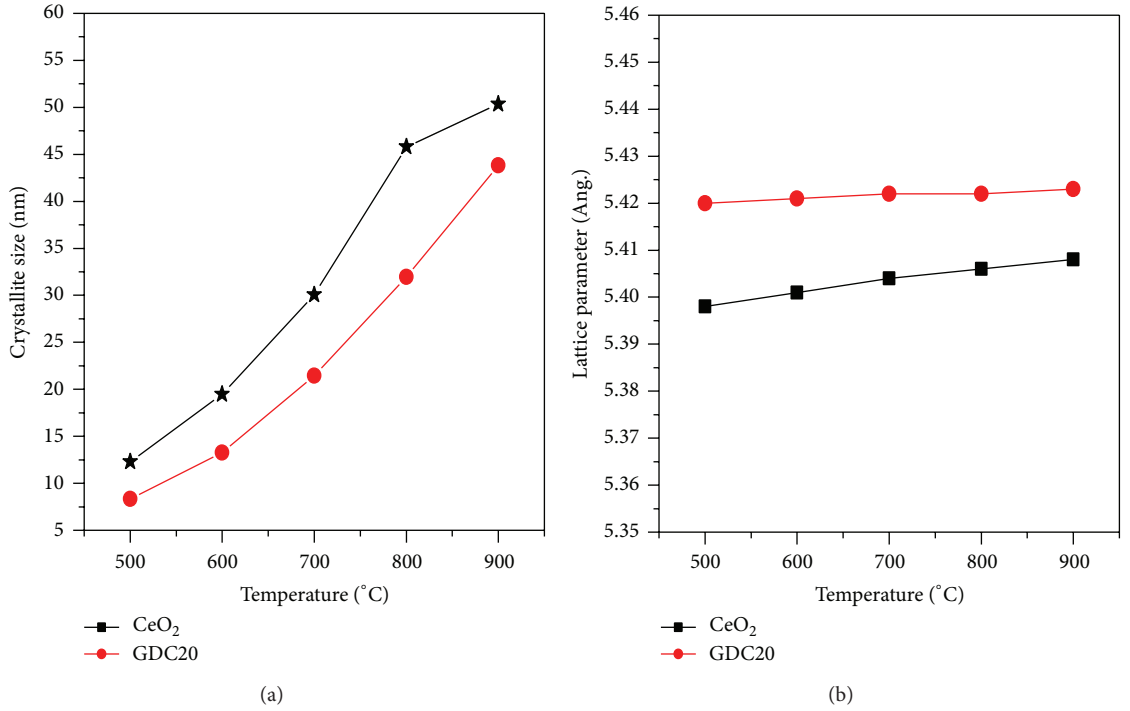

FIGURE 7: (a) The average crystallite size of CeO_2 and GDC20 nanofibers, which were measured from X-ray line broadening and (b) the lattice parameter of CeO_2 and GDC20 nanofibers calcined at 500–900°C for 8 h in air.

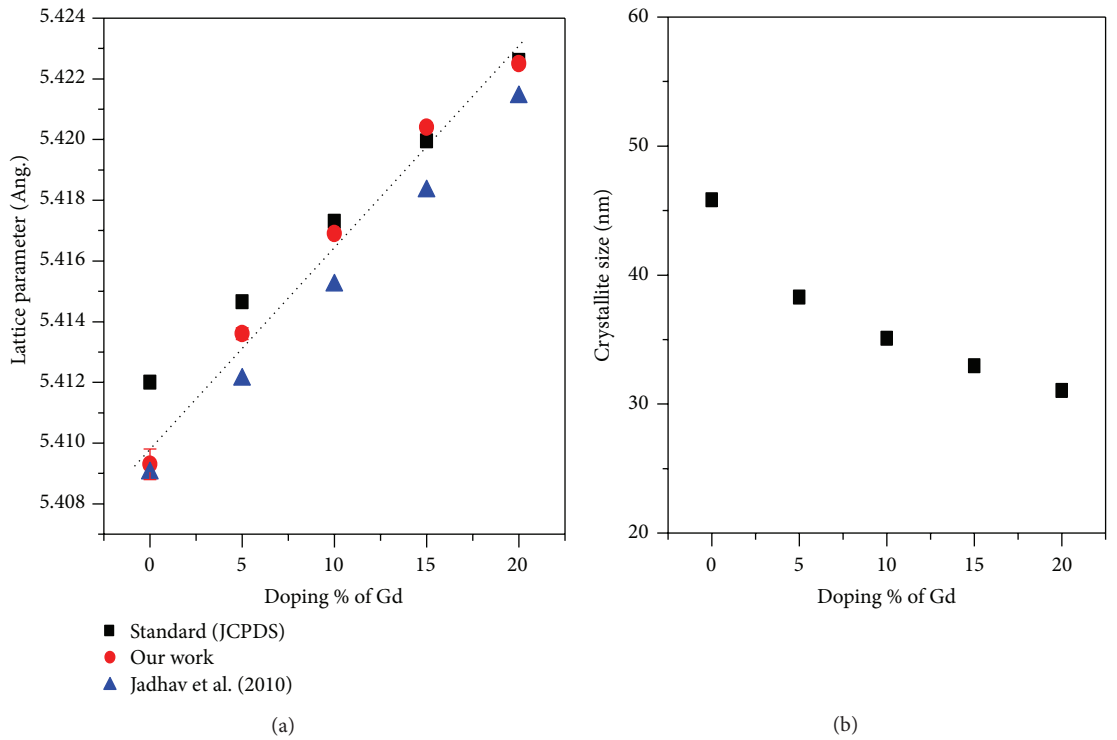

FIGURE 8: (a) The lattice parameter of GDCX (X = 0–20%) obtained from a JCPDS database, Jadhav et al. (2010) and our work. (b) The average crystallite size of GDCX (X = 0–20%) calcined at 800°C for 8 h in air.

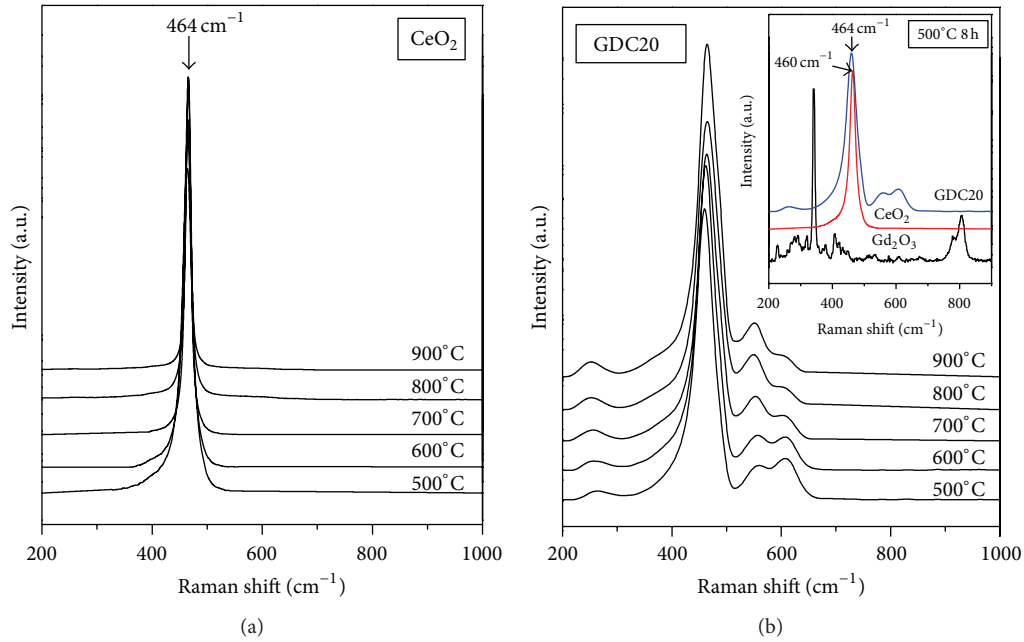

FIGURE 9: Raman spectra of (a) CeO_2 and (b) GDC20 nanofibers calcined at 500–900°C for 8 h in air.

more ordered oxygen in the bulk, resulting in the reduction of GdO_8-type defect complex.

3.8. EIS Analysis. The total resistances of GDC20 pellets sintered at 1400°C for 4 h were taken from the intercept of real impedance which includes both grain and grain boundary resistance. The resistance result was then converted to the total conductivity using a simple equation below:

$$\sigma = \frac{L}{AR}, \tag{2}$$

where σ is a total conductivity, L is a sample thickness, A is an electrode area, and R is a sample resistance. The average thickness of pressed GDC20 samples is ~0.064 cm. Though these samples are rather thin, they are mechanically stable enough for the conductivity testing which requires certain strength to withstand the spring force that presses the current collector onto the sample. The conductivity was measured at 250–800°C with 25°C interval. From Figure 10, two linear fits are clearly implicative in the Arrhenius plot; that is, one line goes from 250 to 500°C and the other extends from 550 to 750°C. The first set of slope occurring at the lower temperature range is associated with the enthalpy of migration of oxygen ions (ΔH_m), the association enthalpy of complex defects (ΔH_a), and the activation energy for the GB conduction (E_{gb}) [25]. For the high temperature range, only ΔH_m plays the major role in dictating the total conductivity value. The total activation energy of our GDC20 at the lower temperature range and the higher temperature one is 1.13±0.02 eV and 0.65±0.02 eV, respectively. At the low temperature range, when compared to Zhang et al. [25], our GDC20 conductivity is poorer because of its higher activation energy; however, our results at the higher temperature range are comparable theirs since the activation energy value of

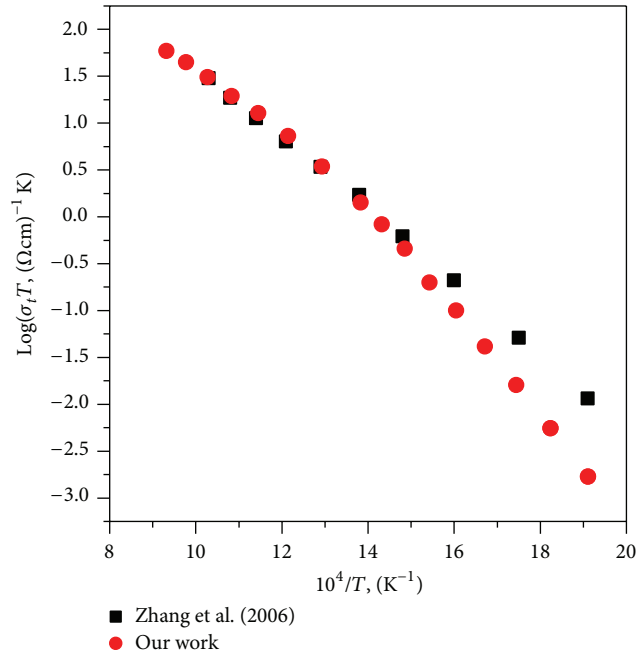

FIGURE 10: Arrhenius plots of the total conductivity (σ_t) GDC20 in air of our work (■) as compared to that of Zhang et al. (2006) (●).

our GDC20 becomes lower. The complex defects and grain boundary impurities in the GDC20 sample could be the major factors in increasing the total enthalpy at the lower temperature range, so the total conductivity is significantly reduced. From our results, the GDC20 prepared from the polymerization complex method is still suitable to be used at 600°C, which still falls within the workable intermediate temperature seeing that their conductivities exceed 0.01 S/cm.

4. Conclusions

The hollow nanofibers of $Ce_{0.8}Gd_{0.2}O_{2-\delta}$ were directly fabricated by an electrospinning technique. The existence of hollow core was confirmed by FESEM and TEM. The nanocores majorly form during the disintegration stage of polymer matrix and the crystallization of the nano-GDC20. For nanofibers heated at 250–300°C, increasing temperature results in less time required for the hollow structure to form. The closure of the hollow core was observed at 900°C. The average outer diameters of calcined nanofibers vary from 87.25 to 51.85 nm. XRD and Raman analysis confirm the successful doping of Gd for the GDC20 sample, resulting in the conductivity of above 0.01 S/cm at 600°C.

Conflict of Interests

The authors declare that they have no conflict of interests regarding the publication of this paper.

Acknowledgments

This work was financially supported by the Higher Education Research Promotion and National Research University Project of Thailand, Office of the High Education Commission, through the Advance Functional Materials Cluster of Khon Kaen University, and the Integrated Nanotechnology Research Center (INRC), Khon Kaen University, Thailand. This work has also been partially supported by the National Nanotechnology Center (NANOTEC), NSTDA, Ministry of Science and Technology, Thailand, through its program of Center of Excellence Network. More fundings were also obtained from Biosensing Technology for Sustainable Development Research Group, Khon Kaen University, Thailand, and Thailand Center of Excellence in Physics, CHE, Ministry of Education, Bangkok, Thailand.

References

[1] H. Inaba and H. Tagawa, "Cerai-bassed solid eletrolytes," *Solid State Ionics*, vol. 83, no. 1-2, pp. 1–16, 1996.

[2] P. Jasinski, T. Suzuki, and H. U. Anderson, "Nanocrystalline undoped ceria oxygen sensor," *Sensors and Actuators B*, vol. 95, no. 1–3, pp. 73–75, 2003.

[3] A. Hadi and I. I. Yaacob, "Synthesis of PdO/CeO_2 mixed oxides catalyst for automotive exhaust emissions control," *Catalysis Today*, vol. 96, no. 3, pp. 165–170, 2004.

[4] B. Choudhury and A. Choudhury, "Ce^{3+} and oxygen vacancy mediated tuning of structural and optical properties of CeO_2 nanoparticles," *Materials Chemistry and Physics*, vol. 131, no. 3, pp. 666–671, 2012.

[5] W. Y. Hernández, O. H. Laguna, M. A. Centeno, and J. A. Odriozola, "Structural and catalytic properties of lanthanide (La, Eu, Gd) doped ceria," *Journal of Solid State Chemistry*, vol. 184, no. 11, pp. 3014–3020, 2011.

[6] H. Yokokawa, T. Horita, N. Sakai et al., "Ceria: relation among thermodynamic, electronic hole and proton properties," *Solid State Ionics*, vol. 177, no. 19–25, pp. 1705–1714, 2006.

[7] L. D. Jadhav, M. G. Chourashiya, A. P. Jamale, A. U. Chavan, and S. P. Patil, "Synthesis and characterization of nano-crystalline $Ce_{1-x}Gd_xO_{2-x/2}$ ($x = 0 - 0.30$) solid solutions," *Journal of Alloys and Compounds*, vol. 506, no. 2, pp. 739–744, 2010.

[8] M. G. Chourashiya and L. D. Jadhav, "Synthesis and characterization of 10%Gd doped ceria (GDC) deposited on NiO-GDC anode-grade-ceramic substrate as half cell for IT-SOFC," *International Journal of Hydrogen Energy*, vol. 36, no. 22, pp. 14984–14995, 2011.

[9] A. Atkinosn, "Chemically-induced stresses in gadolinium-doped ceria solid oxide fuel cell electrolytes," *Solid State Ionics*, vol. 95, no. 3-4, pp. 249–258, 1997.

[10] Z. P. Li, T. Mori, F. Ye, D. R. Ou, J. Zou, and J. Drennan, "Dislocation associated incubational domain formation in lightly gadolinium-doped ceria," *Microscopy and Microanalysis*, vol. 17, no. 1, pp. 49–53, 2011.

[11] C. Xia and M. Liu, "Microstructures, conductivities, and electrochemical properties of $Ce_{0.9}Gd_{0.1}O_2$ and GDC-Ni anodes for low-temperature SOFCs," *Solid State Ionics*, vol. 152-153, pp. 423–430, 2002.

[12] R. O. Fuentes and R. T. Baker, "Synthesis and properties of Gadolinium-doped ceria solid solutions for IT-SOFC electrolytes," *International Journal of Hydrogen Energy*, vol. 33, no. 13, pp. 3480–3484, 2008.

[13] J. Y. Yu, W. C. Wei, S. E. Lin, and J. M. Sung, "Synthesis and characterization of cerium dioxide fibers," *Materials Chemistry and Physics*, vol. 118, no. 2-3, pp. 410–416, 2009.

[14] S. Dikmen, P. Shuk, M. Greenblatt, and H. Gocmez, "Hydrothermal synthesis and properties of $Ce_{1-x}Gd_xO_{2-\delta}$ solid solutions," *Solid State Sciences*, vol. 4, no. 5, pp. 585–590, 2002.

[15] A. M. Azad, T. Matthews, and J. Swary, "Processing and characterization of electrospun Y_2O_3-stabilized ZrO_2 (YSZ) and Gd_2O_3-doped CeO_2 (GDC) nanofibers," *Materials Science and Engineering B*, vol. 123, no. 3, pp. 252–258, 2005.

[16] D. Li and Y. Xia, "Direct fabrication of composite and ceramic hollow nanofibers by electrospinning," *Nano Letters*, vol. 4, no. 5, pp. 933–938, 2004.

[17] S. Zhan, D. Chen, X. Jiao, and C. Tao, "Long TiO_2 hollow fibers with mesoporous walls: Sol-gel combined electrospun fabrication and photocatalytic properties," *Journal of Physical Chemistry B*, vol. 110, no. 23, pp. 11199–11204, 2006.

[18] C. Qizheng, D. Xiangting, W. Jinxian, and L. Mei, "Direct fabrication of cerium oxide hollow nanofibers by electrospinning," *Journal of Rare Earths*, vol. 26, no. 5, pp. 664–669, 2008.

[19] T. Wang and D.-C. Sun, "Preparation and characterization of nanometer-scale powders ceria by electrochemical deposition method," *Materials Research Bulletin*, vol. 43, no. 7, pp. 1754–1760, 2008.

[20] A. Vantomme, Z. Y. Yuan, G. Du, and B. L. Su, "Surfactant-assisted large-scale preparation of crystalline CeO_2 nanorods," *Langmuir*, vol. 21, no. 3, pp. 1132–1135, 2005.

[21] M. G. Chourashiya, J. Y. Patil, S. H. Pawar, and L. D. Jadhav, "Studies on structural, morphological and electrical properties of $Ce_{1-x}Gd_xO_{2-(x/2)}$," *Materials Chemistry and Physics*, vol. 109, no. 1, pp. 39–44, 2008.

[22] T. Taniguchi, T. Watanabe, N. Sugiyama et al., "Identifying defects in ceria-based nanocrystals by UV resonance Raman spectroscopy," *Journal of Physical Chemistry C*, vol. 113, no. 46, pp. 19789–19793, 2009.

[23] M. J. Godinho, R. F. Gonçalves, L. P. S Santos, J. A. Varela, E. Longo, and E. R. Leite, "Room temperature co-precipitation of nanocrystalline CeO_2 and $Ce_{0.8}Gd_{0.2}O_{1.9-\delta}$ powder," *Materials Letters*, vol. 61, no. 8-9, pp. 1904–1907, 2007.

[24] L. Li, F. Chen, J. Q. Lu, and M. F. Luo, "Study of defect sites in $Ce_{1-x}M_xO_{2-\delta}$ ($x = 0.2$) solid solutions using raman spectroscopy," *Journal of Physical Chemistry A*, vol. 115, no. 27, pp. 7972–7977, 2011.

[25] T. S. Zhang, J. Ma, H. Cheng, and S. H. Chan, "Ionic conductivity of high-purity Gd-doped ceria solid solutions," *Materials Research Bulletin*, vol. 41, no. 3, pp. 563–568, 2006.